Radboud Repository

Radboud University Nijmegen

PDF hosted at the Radboud Repository of the Radboud University Nijmegen

The following full text is a preprint version which may differ from the publisher's version.

For additional information about this publication click this link.
http://hdl.handle.net/2066/166083

Please be advised that this information was generated on 2017-12-05 and may be subject to change.

Journal Name

ARTICLE TYPE

Cite this: DOI: 10.1039/xxxxxxxxxx

Degradation mechanism(s) of GaAs solar cells with Cu contacts

R. H. van Leest [a*], K. de Kleijne [a], G. J. Bauhuis [a], P. Mulder [a], H. Cheun [b], H. Lee [b], W. Yoon [b], R. van der Heijden [c], E. Bongers [c], E. Vlieg [a], and J. J. Schermer [a]

Received Date
Accepted Date

DOI: 10.1039/xxxxxxxxxx

www.rsc.org/journalname

Substrate-based GaAs solar cells having a dense Au/Cu front contact grid with 45% surface coverage were exposed to accelerated life testing at temperatures between 200 and 300°C. TEM analysis of the front contacts was used to gain a better understanding of the degradation process. During accelerated life testing at 200°C only intermixing of the Au and Cu in the front contact occurs, without any significant influence on the J-V curve of the cells, even after 1320h (55 days) of accelerated life testing. At temperatures $\geq$ 250°C a recrystallization process occurs in which the metals of the contact and the GaAs front contact layer interact. Once the grainy recrystallized layer starts to approach the window, diffusion via grain boundaries to the window and into the active region of the solar cells occurs, causing a decrease in V_{oc} due to enhanced non-radiative recombination via Cu trap levels introduced in the active region of the solar cell. To be a valid simulation of space conditions the accelerated life testing temperature should be $<$ 250°C in future experiments, in order to avoid recrystallization of the metals with the GaAs contact layer.

1 Introduction

In recent years thin-film, III-V solar cells prepared by the epitaxial lift-off (ELO) technique [1,2] have displayed their potential by demonstrating efficiencies equal to those of cells on a growth substrate [3,4]. As a result of photon confinement [5,6] efficiencies even exceeding those of cells on their native epitaxial growth substrate can be obtained [7,8]. Such flexible, high-efficiency, thin-film solar cells find a potential application in solar panels for space missions [9], where launch costs can be significantly reduced due to the lower weight of thin-film panels. The replacement of the expensive growth substrate with a flexible carrier can reduce the weight by approximately 25% on cell level. Additional weight reduction can be accomplished by replacing the rigid cover glass with a flexible coating [10,11] and implementing a new lightweight support to replace the currently used rigid aluminium honeycomb support. In theory this allows for a total weight reduction of more than 75% [11]. Additional cost reductions are possible since ELO allows for re-use of the expensive growth substrates [12,13] and there is the possibility to grow multiple devices on the same wafer and peeling them off separately one by one [14,15].

[a] *Radboud University, Institute for Molecules and Materials, Heyendaalseweg 135, 6525 AJ Nijmegen, The Netherlands*

[*] *Corresponding author, e-mail: L.vanLeest@science.ru.nl*

[b] *LG Electronics Materials & Devices Advanced Research Institute, 16 Woomyeon-Dong, Seocho-Gu, Seoul 137-724, Korea*

[c] *Airbus Defence and Space Netherlands B.V., Mendelweg 30, 2333 CS Leiden, The Netherlands*

However, space is an extreme environment (for example high vacuum, harsh UV irradiation, charged particle radiation, atomic oxygen and thermal cycling [16]), which provides additional challenges in solar panel design. One of these concerns the flexible carrier for the solar cells. The thin-film cells might be mounted on a plastic substrate. However, plastics and glues are primarily made of organic polymers, which are known to be mostly incompatible with the space environment [10,11]. Another option is the use of a flexible metal foil carrier, for which copper is the favoured choice [12,17,18], as it is both relatively cheap and chemically resistant in post ELO processing.

Nevertheless copper also poses a potential risk, as it is known to be a fast diffuser in many semiconductors [19–27] and tends to create a mid band gap trap level [28]. These two characteristics have a potentially detrimental effect on solar cell performance. Unfortunately, most of the available literature describes copper diffusion in bulk semiconductor material at high temperatures ($>$ 500°C). There is only limited literature available on the effects of copper in actual devices and it mostly describes the effects of deliberate copper doping or contamination [29–32], rather than the effect of gradual diffusion over time.

In addition to the potentially harmful effect of copper diffusion, interaction between the Cu carrier, the Au contact and the GaAs contact layer may affect solar cell degradation as well. The Au-Cu phase diagram shows that Au and Cu may form Au_3Cu, AuCu and $AuCu_3$ at temperatures below 410°C [33]. Interaction between GaAs and Au is unlikely to occur according to Tsai and Williams [34]

This journal is © The Royal Society of Chemistry [year]

and the calculated phase diagram of Cu and GaAs shows that Ga_xCu_y and Cu_aAs_b compounds may be formed[35]. Unfortunately, calculating or predicting how GaAs, Au and Cu interact at various temperatures and gradually over time is complex if at all possible, as it is difficult to predict which compounds form at what temperatures.

With space applications in mind, it is important to gain a better understanding of gradual copper diffusion in III-V semiconductor devices and interactions between the contact metals and the semiconductor materials in order to reveal the underlying mechanisms which ultimately result in device failure. Better understanding of the degradation mechanisms is required to be able to develop optimal solutions for, or alternatives to, the Cu foil carrier.

Out of the harsh conditions encountered in space high energy particle irradiation and temperature cycling might be expected to be relevant for the diffusion process, as high energy particle irradiation induces defects[36] and the diffusion is expected to depend on the presence of defects such as vacancies[21] and diffusion is temperature dependent. In a previous study[37] it was found that heat treatments indeed induce Cu diffusion, but no influence of electron irradiation on the diffusion process was observed. Therefore subsequent research was focussed primarily on investigating the temperature dependent degradation mechanism(s) causing solar cell degradation as a result of copper diffusion.

As the thin-film ELO solar cells eventually have to operate properly for at least 10 to 15 years in space, an accelerated ageing process is necessary to speed up the diffusion process for testing purposes. Since diffusion is exponentially dependent on temperature ($D=D_0\exp(-E_a/kT)$), accelerated life testing (ALT) offers a suitable approach. ALT assumes that operation for a long period of time at a relatively low temperature is equal to operation for a short period of time (few hours) at a higher temperature. This can be described with the following equation[38]:

$$\frac{t_{op}}{t_{acc}} = \exp\left[\frac{E_a}{k}\left(\frac{1}{T_{op}} - \frac{1}{T_{acc}}\right)\right], \qquad (1)$$

in which k is the Boltzmann constant, E_a the activation energy, T_{op} the regular operation temperature, T_{acc} the accelerated test temperature and t_{op} and t_{acc} the exposure times to the corresponding temperatures. The main difficulty with this generally applied method is that activation energy determination is difficult and hence there are very few activation energies reported for solar cell degradation[38–41] and none of these concerns (Cu) diffusion. The European Cooperation for Space Standardization (ECSS) standard for photovoltaic assemblies and components (ECSS-E-ST-20-08C[42]) advises to use an E_a of 0.70 eV in calculations. For an accelerated test temperature of 300°C this results in accelerated test times of 10, 44 and 66 hours for simulation of a Geosynchronous orbit mission (GEO,15 years, max 70°C), a Low-Earth orbit mission (LEO, 10 years, max 100°C) and an extreme scenario (15 years, max 100°C) respectively. At lower test temperatures the test time rapidly increases to several days, while at higher test temperatures the risk of cell failure due to other effects increases. This study utilizes initial ALT of 4h at 300°C, which covers all three scenarios (GEO, LEO and extreme) if the more optimistic E_a of 1.02eV reported in a study conducted by Nuñez et. al[38] is used. Subsequently the test could be extended to 10, 44 or 66 hours in further experiments whenever required[37].

Unfortunately ELO cells appear to be incompatible with the accelerated ageing test at temperatures $\geq$ 200°C[37]. This is most likely due to the significant differences in thermal expansion coefficient between the GaAs solar cell ($5.4 \cdot 10^{-6}K^{-1}$) on the one hand and gold ($14.2 \cdot 10^{-6}K^{-1}$) and copper ($16.5 \cdot 10^{-6}K^{-1}$) contact/carrier on the other, which eventually causes stress and cracks in the semiconductor. Therefore an adapted substrate based cell design has been developed[37]. In the normal ELO thin-film cells the copper foil is applied at the back. This is not a suitable choice for the substrate based cells as the copper would have to diffuse through a few hundred microns of substrate before reaching the active region of the solar cell. Thus the copper has to be applied on the front contact of the solar cells. However, the front contact grid typically covers only a few percent of the surface, which is not comparable to the fully covered back surface in an ELO cell. As it is also not possible to cover the front surface completely with copper (light would no longer be able to enter the cell), a grid pattern with 45% coverage was used for the front contact. This allows for proper operation of the device and at the same time places a sufficient fraction of the active cell structure in close contact with a copper layer.

In order to elucidate the failure mechanism of GaAs solar cells with copper metallization, several accelerated life tests were performed. Based on the evaluation of the cell performance by J-V measurements and TEM analysis of the cells, a low temperature and a high temperature degradation mechanism of the copper contacts are proposed in this study.

300nm	$5.0 \cdot 10^{18}$ cm^{-3} Si-doped	n-GaAs	contact layer
20nm	$4.0 \cdot 10^{17}$ cm^{-3} Si-doped	n-$Al_{0.53}In_{0.47}P$	window
75nm	$3.0 \cdot 10^{18}$ cm^{-3} Si-doped	n-GaAs	emitter
2000nm	$1.0 \cdot 10^{17}$ cm^{-3} Zn-doped	p-GaAs	base
70nm	$5.0 \cdot 10^{17}$ cm^{-3} Zn-doped	p-$In_{0.48}Ga_{0.52}P$	BSF
300nm	$1.5 \cdot 10^{18}$ cm^{-3} Zn-doped	p-GaAs	contact layer
~350µm	$2.x \cdot 10^{19}$ cm^{-3} Zn-doped	p-GaAs	substrate

Fig. 1 Schematic representation of the solar cell structure.

2 Materials and methods

Solar cell structures as depicted in figure 1 were grown in an Aixtron 200 MOCVD reactor on 2 inch Zn-doped p-type GaAs substrates ((1 0 0) 2° off towards [1 1 0]). An Au/Cu front grid contact with 45% surface coverage (see figure 2) was applied us-

This journal is © The Royal Society of Chemistry [year]

ing photolithography and e-beam evaporation. The Au layer was kept at a constant thickness of 100nm while the thickness of the copper layer was varied between 0 and 1000nm. After metallization 6mm x 6mm solar cells were created using a MESA etch. A 1:2:10 NH_4OH:H_2O_2:H_2O etch was used for the GaAs layers and a 37% HCl etch for the AlInP and InGaP layers. Then the contact layer between the grid fingers was etched away with a 2:1:10 NH_4OH:H_2O_2:H_2O etch, while the front contact grid was protected by a photoresist layer. Finally a ZnS (42.5nm) / MgF_2 (88.0nm) anti-reflection coating (blue square in figure 2) was applied by e-beam evaporation. Subsequently all solar cells were characterized by J-V measurements at 25°C under 1 sun AM1.5 illumination using an Abet Sun 2000 solar simulator in combination with Tracer 3.0 software from ReRa solutions.

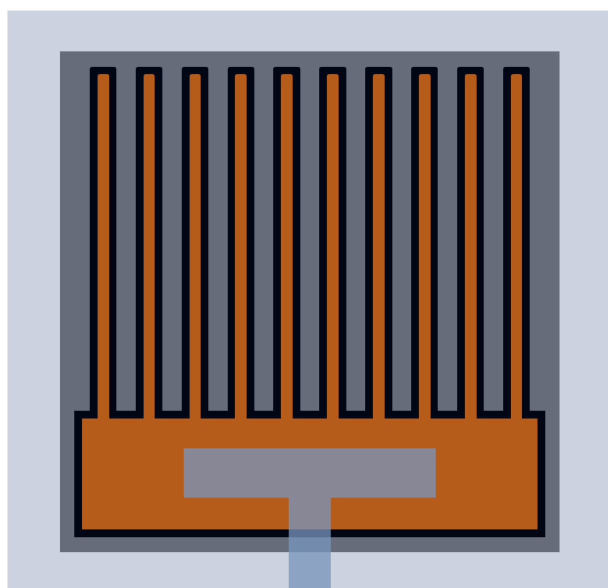

Fig. 2 Schematic depiction of the front surface of the solar cell. The dark grey square indicates the actual 6mm x 6mm solar cell, the orange pattern is the metal front contact grid consisting of a 1.66mm x 5.76mm bar with ten 4.08mm x 160μm grid fingers, the black area indicates the remainder of the n-GaAs contactlayer (1.7mm x 5.8mm bar with 4.1mm x 200μm grid fingers). The blue square indicates the anti reflection coating (ARC), with the blue t-shape representing the contact pad without ARC.

Sets of two solar cells were exposed to ALT in a N_2 atmosphere in either a rapid thermal annealing (RTA) furnace or a tube oven. In the RTA furnace the cells were exposed to a temperature of 200, 250 or 300°C for a stepwise increasing time (4 x 15 minutes followed by 6 x 30 minutes) up to a total of 4h. In the tube oven the cells were exposed to a temperature of 300°C for 4h. With sets of 3 cells a stepwise long duration experiment (steps of 88h, 128h, 672 and 432h) was conducted in a vacuum oven at 200°C for a total of 1320h (55 days). Assuming E_a equals 0.70eV the first step equals 4h at 300°C, step 1 and 2 a GEO mission, step 1, 2 and 3 a LEO mission and all four steps the extreme scenario of 15 years at 100°C.

After each ALT step the cells were again characterized by J-V measurements. No significant differences in results were observed between cells annealed stepwise up to a total of 4 hours in the RTA furnace and cells annealed in a single step of 4 hours in the tube oven.

Based on the results of the ALT, cells were selected for transmission electron microscopy (TEM) analysis. These solar cells were covered with a thin Pt protection layer. A cross-section was made and then thinned using focused ion beam milling to allow for cross-sectional TEM analysis of the front contacts. TEM images were obtained with a FEI Titan G2 microscope equipped with EDX analysis tools to determine the composition of the visualized structures.

3 Results and Discussion

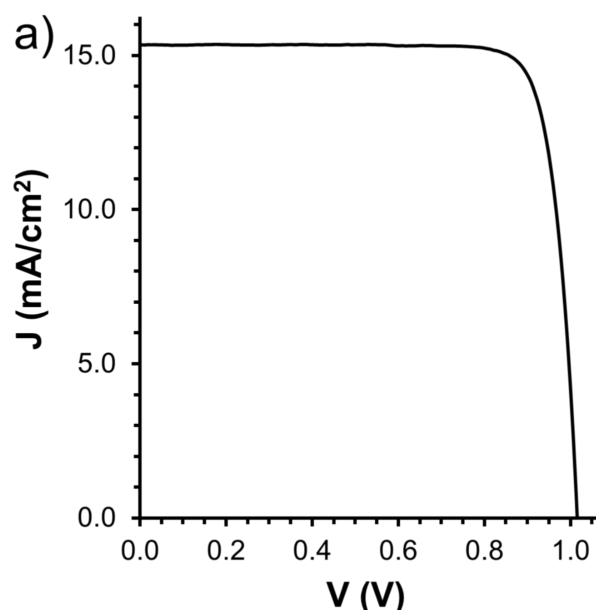

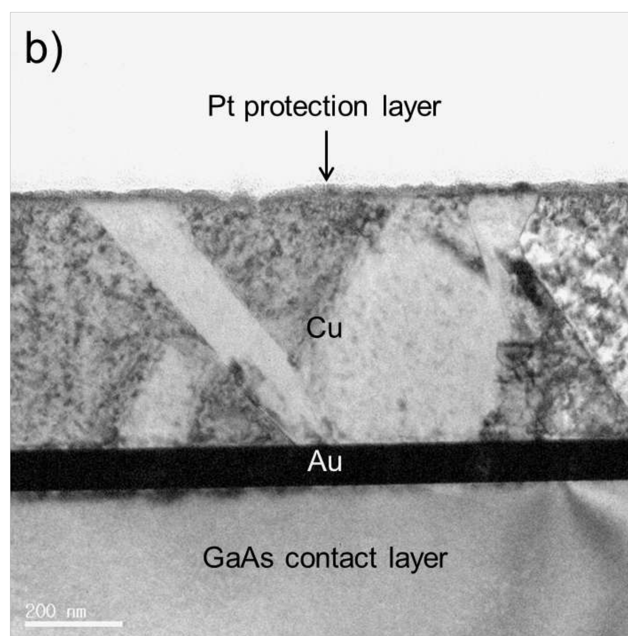

Fig. 3 a) J-V curve and b) TEM image of the Au (100nm) / Cu (500nm) front contact of a cell before ALT.

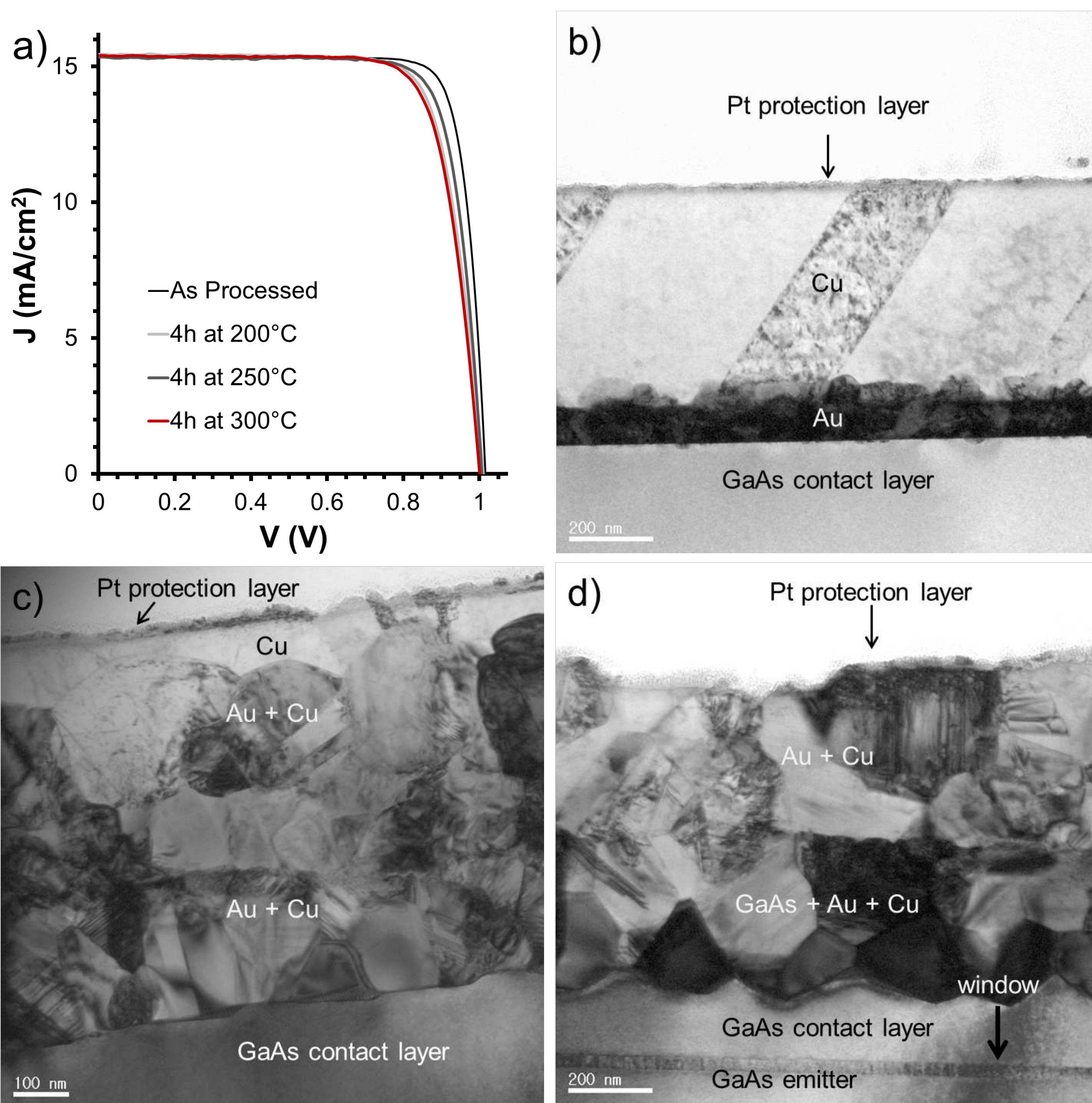

Fig. 4 a) J-V curves and b-d) TEM images of the front contact for cells before ALT (black curve), as well as after ALT of 4h at 200°C (light grey curve, image b), 250°C (dark grey curve, image c) and 300°C (red curve, image d).

3.1 Transmission electron microscopy

In figure 3 the J-V curve of an as processed cell (i.e. not subjected to ALT) with an Au (100nm) / Cu (500nm) front contact and a TEM image of the front contact of the same cell are shown. With a short-circuit current density J_{sc} (current at zero voltage) of 15.3mA/cm^2, an open-circuit voltage V_{oc} (voltage at zero current density) of 1015mV and a fill factor (measure for the squareness of the curve) of 83.4% the as processed cell has excellent J-V characteristics (see figure 3a). J_{sc} may appear to be low (typical values being in the order of 25-30mA/cm^2), but this is only related to the 45% coverage of the front contact. The TEM image in figure 3b shows that the front contact in the as processed cell consists of well defined GaAs, Au and Cu layers, with smooth interfaces between them. The mono-crystalline GaAs contact layer shows no distinct features. The gold layer appears quite dark, but shows some slightly lighter coloured areas suggesting the presence of a multi-crystalline material. The colour differences in the Cu layer indicate that several large Cu domains with different orientation are present.

The effect of increasing ALT temperatures on the front contact is illustrated in figure 4. In figures 4b-4d TEM images of the front contact after 4h ALT at respectively 200, 250 and 300°C are shown. In figure 4a the J-V curves of these cells are plotted together with the J-V curve of an as processed cell. Although the differences in the J-V curves after ALT are small, the TEM images

This journal is © The Royal Society of Chemistry [year]

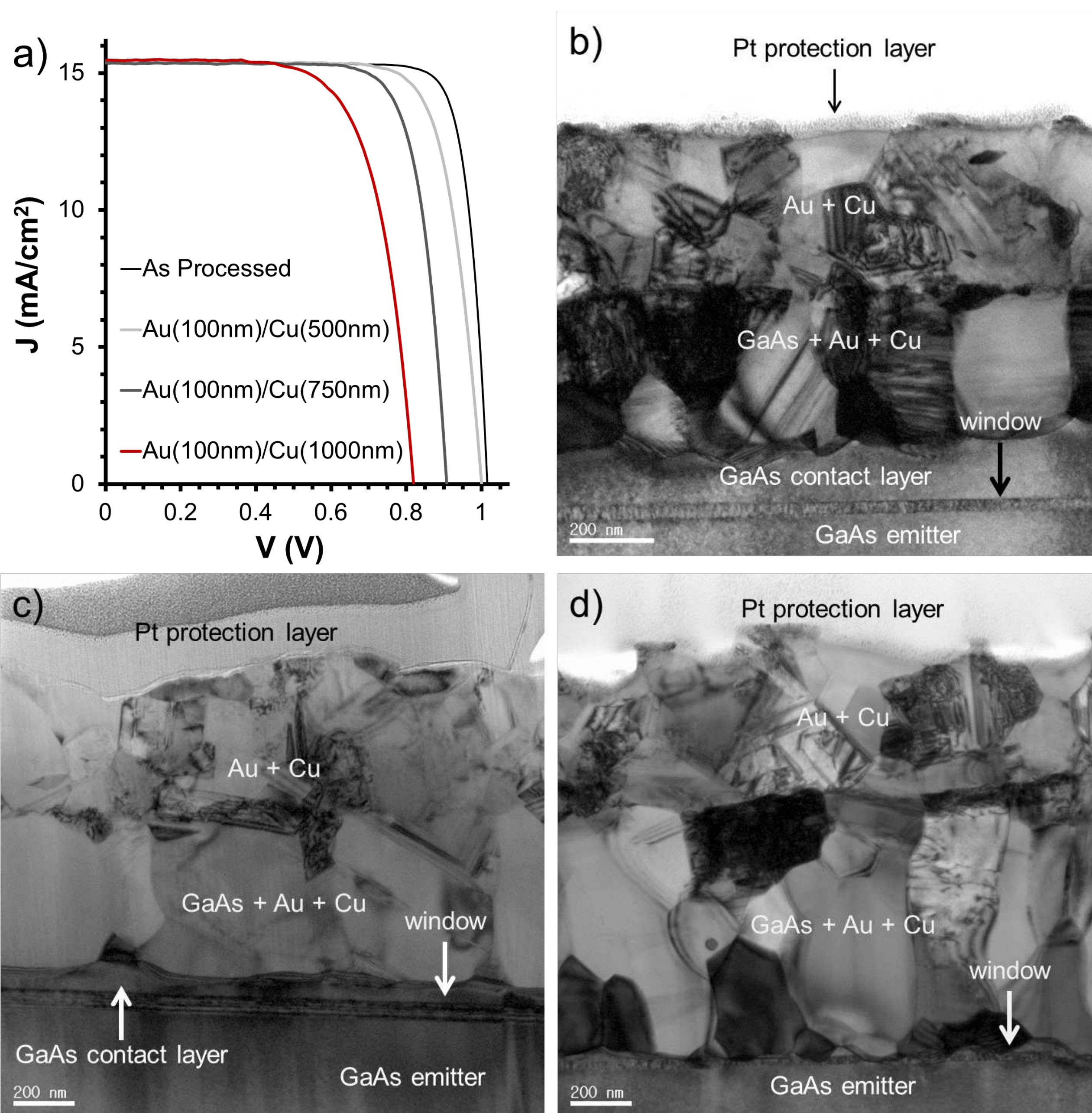

Fig. 5 a) J-V curves and b-d) TEM images of the front contact for cells before ALT (black curve), as well as after ALT for 4h at 300°C for a cell with 500nm Cu in the front contact (light grey curve, image b), 750nm Cu in the front contact (dark grey curve, image c) and 1000nm Cu in the front contact (red curve, image d).

in figures 4b-4d show a huge transformation in the morphology of the front contacts. After 4h ALT at 200°C the contact morphology (see figure 4b) is only slightly different compared to that of the as processed cell (see figure 3b). The interface between Au and Cu is no longer smooth and some grains appear to have formed at the interface, while the Au-GaAs interface is still intact and the Cu domains in the Cu layer are still visible. After ALT at 250°C (see figure 4c) only a small part of the polycrystalline Cu layer remains, while the largest part of it, together with the Au layer, now have formed a grainy structure in which the individual Au and Cu layers are no longer distinguishable. The interface between the metal and GaAs appears slightly less smooth, though the GaAs contact layer is not noticeably thinner. EDX analysis (not shown here) indicates that there are traces of As present at the bottom of the metal layer, indicating that interaction between the metals and the GaAs starts to occur. After 4h ALT at 300°C the entire Cu layer has disappeared, the interface between the GaAs contact layer and the metals has become undulated and the GaAs contact layer is on average only 160nm thick. Hence part of the GaAs contact layer has interacted with the metals, which is confirmed by the EDX measurements.

The effect of increasing Cu thickness on the front contact is illustrated in figure 5. In figures 5b-5d TEM images of the front contacts after 4h ALT at 300°C are shown for cells with respec-

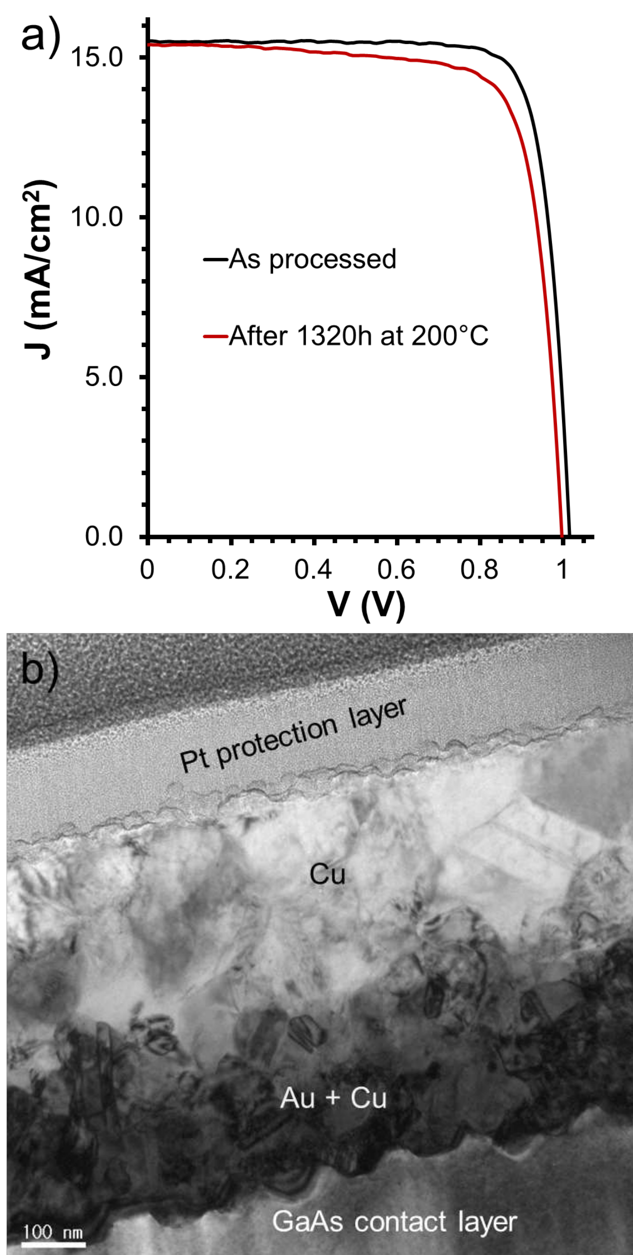

Fig. 6 For a cell with Au (100nm) / Cu (500nm) front contact a) J-V curves of the as processed cell (black curve) and after an ALT of 1320h (red curve) at 200°C and b) a TEM image of the front contact after an ALT of 1320h at 200°C.

tively 500, 750 and 1000nm Cu in the front contact. The J-V curves of these cells are plotted together with the curve of an as processed cell in figure 5a. The TEM pictures in figures 5b-5d show an interesting trend. For the cell with an Au (100nm) / Cu (500nm) front contact after ALT (see figure 5b), the Au and Cu have interacted with the GaAs contact layer as the latter is significantly thinner (∼140nm) than the 300nm that was deposited during cell growth (note that figures 4d and 5b are images from different cells). For the cell with 750nm Cu in the front contact (see figure 5c) the GaAs layer thickness has decreased to only ∼50nm and for the cell with 1000nm Cu in the front contact (see 5d) the recrystallized Au-Cu-GaAs layer extends all the way to the window and at some places it even seems to protrude the window. The window is implemented to minimize surface recombination of minority carriers, large surface recombination rates cause a reduction in J_{sc}. As J_{sc} does not decrease, it seems unlikely that the recrystallized layer actually penetrated through the window.

Combining the information from J-V and TEM analysis it appears that once the recrystallized layer starts to approach the window the V_{oc} starts to drop. As the recrystallized layer introduces additional grain boundaries which are known to be very efficient diffusion pathways[43] it seems reasonable to assume that due to recrystallization Cu atoms can diffuse rapidly from the top of the contact (almost) to the window layer. From there the Cu atoms can diffuse into the active region of the cell, where they introduce trap levels which cause a reduction in V_{oc}. The window appears to block the recrystallization process, but the decrease in V_{oc} shows that Cu diffusion can still proceed.

It is now interesting to see what the effects of long ALT at low (200°C) temperature are. In figure 6a the J-V curves are plotted for an as processed cell with 500nm Cu in the front contact and of the same cell after 1320h of ALT at 200°C. In figure 6b the TEM image of the front contact of the 500nm Cu cell after 1320h ALT at 200°C is shown. Figure 6a shows that upon ALT J_{sc} remains constant at 15.4-15.5mA/cm^2, that V_{oc} decreases a little from 1015mV to 997mV and that FF decreases from 82 to 77%. The shape of the J-V curve shows that the parallel resistance of the sample has decreased. This decrease in parallel resistance is only observed for cells with 5.0*10^{18}cm^{-3} Si-doped front contact layers as used in this study. Additional experiments using cells with differently doped front contact layers (Si- or Te-doped, carrier concentrations between 2.5*10^{18} and 1.6*10^{19}cm^{-3}) exposed to the same test do not show this behaviour. This indicates that the decrease in R_p is not necessarily caused by merely the presence of Cu, but critically depends on the interplay of all the layers of the cell interface.

The TEM image in figure 6b shows intermixing of the Au and Cu layers, but the distinct grainy structure observed after 4h ALT at temperatures ≥250°C has not formed. In this respect the sample shows more resemblance to the cell exposed to 4h ALT at 200°C (see figure 4b). The interface between the Au/Cu and GaAs layers is no longer smooth. As the thickness of the GaAs contact layer is still approximately 300nm (as observed in other TEM images not shown here) only a very small amount of GaAs may have recrystallized with the metals. EDX analysis shows no signs of either Ga or As in the metal layer, indicating that this is indeed the case.

3.2 Degradation mechanism

Based on the TEM images and J-V curves two degradation mechanisms can be distinguished, one that occurs at relatively low ALT temperatures (< 250°C) and one that takes place at higher ALT temperatures (≥250°C). The two mechanisms are schematically depicted in figure 7. Initially, as processed solar cells with Au/Cu front contacts have a contact microstructure that consists of well defined layers of GaAs, Au and Cu with smooth interfaces be-

This journal is © The Royal Society of Chemistry [year]

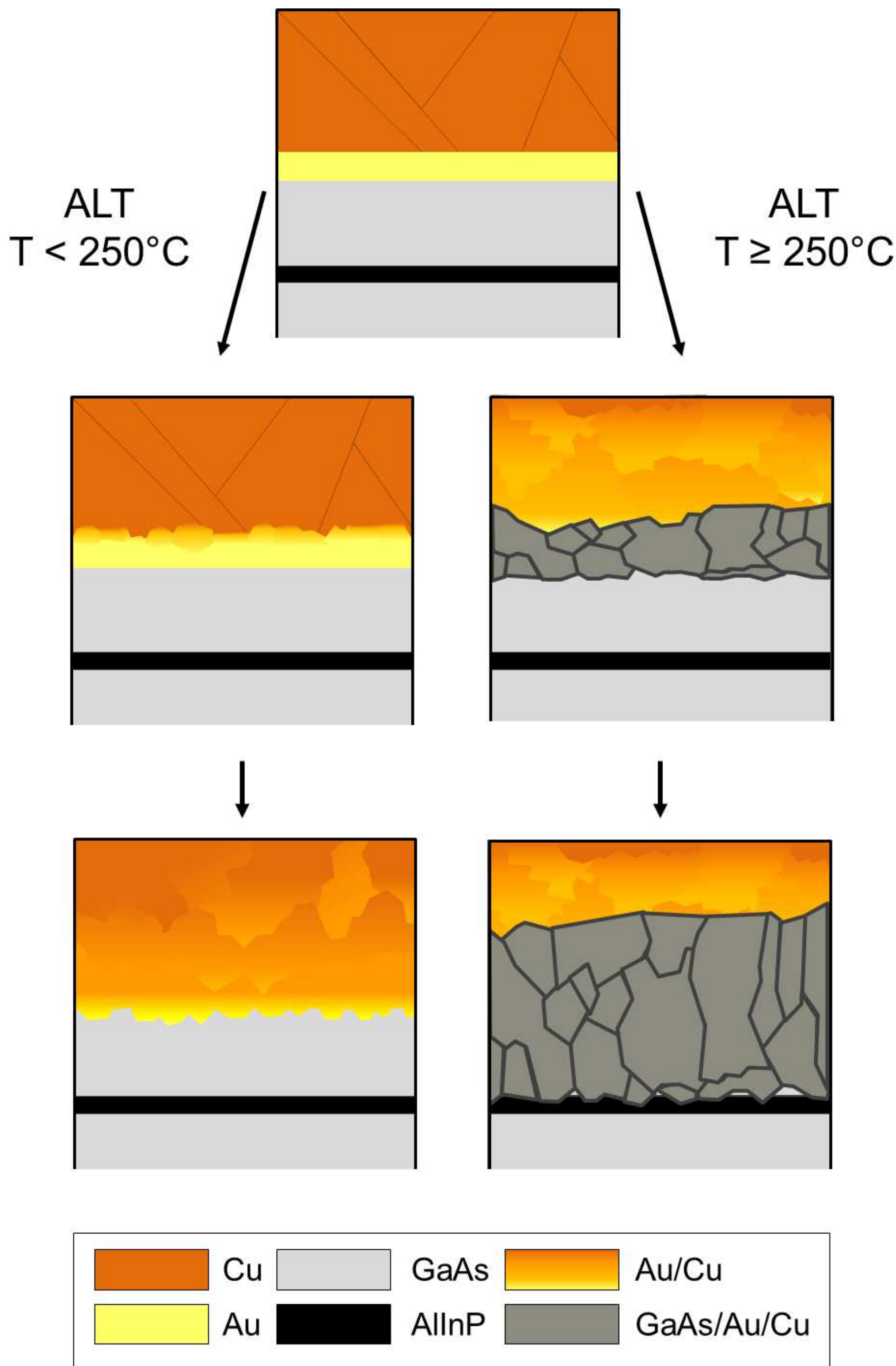

Fig. 7 Schematic representation of the contact degradation mechanisms due to ALT at low temperatures (T<250°C) and at high temperatures (T>250°C).

tween them. The GaAs layer is monocrystalline, the Cu layer is polycrystalline containing large grains with different orientations, the crystallinity of the Au layer cannot be established from the TEM image in figure 3b, but is most likely also polycrystalline.

After ALT at a relatively low temperature (<250°C, see left hand side of figure 7) the Au and Cu layers start to intermix. Initially the Au-GaAs interface remains intact, as well as the majority of the Cu grains. The intermixing of the Au and Cu layers

proceeds with increasing ALT time, eventually resulting in an intermixed Au/Cu layer with a diffuse Cu layer above it. The metal-GaAs interface becomes slightly undulated, but no evidence of recrystallization of the GaAs contact layers with the metals can be found in EDX analysis. The intermixing process has no significant influence on the J-V curve of the solar cell, even after 1320h at 200°C the decrease in V_{oc} is only a few percent, which is similar to the degradation observed for Au contacted cells after the same ALT procedure.

At higher temperatures (≥250°C, see right hand side of figure 7) the intermixing of Au and Cu proceeds more rapidly and eventually a second degradation mechanism starts to occur. Once Cu atoms reach the metal-GaAs interface, Cu starts to recrystallize with the GaAs contact layer. Gradually the contact layer (almost) completely recrystallizes with the contact metals until the recrystallization process is blocked by the AlInP window. The progressing of the recrystallization process coincides with a decrease in the V_{oc} of the solar cells (see figure 5). The recrystallized layer shows a distinct grainy structure with well defined grain boundaries. As grain boundaries are known to be very efficient diffusion pathways[43], any Cu left at the top of the recrystallized layer can diffuse rapidly via these grain boundaries to the remaining contact layer and AlInP window and from there into the active region of the solar cell. There it introduces trap levels which cause the reduction in V_{oc}.

The threshold temperature (∼250°C) observed for the recrystallization process is in agreement with the findings of Kinsbron et. al[44] for Au contacts on (Al)GaAs. They describe a mechanism in which Au starts to alloy with Ga causing As to diffuse out. In the present study EDX analysis of the cells exposed to ALT at 300°C indicate enhanced As concentrations at the top of the contact. Therefore it seems likely that the degradation of Cu/Au/GaAs contacts proceeds by a mechanism similar to the degradation mechanism described for Au/(Al)GaAs.

It appears that rapid Cu diffusion via grain boundaries introduced by recrystallization of Au and Cu with the GaAs contact layer causes a reduction in V_{oc} at ALT temperatures above 250°C. Below this temperature intermixing of the Au and Cu occurs but this process progresses so slowly that even after 1320h (55 days) at 200°C (equal to 15 years at 100°C at an E_a of 0.70eV) no significant reduction in cell performance is observed. Further experiments at 200°C should be conducted with thin-film solar cells in order to investigate whether Cu diffusion really is a problem for application of ELO solar cells in a solar panel for space applications. Potential solutions should be aimed at preventing the intermixing of Au and Cu.

4 Conclusions

In order to gain a better understanding of Cu induced performance degradation, GaAs solar cells with Au/Cu front contacts were exposed to accelerated life testing (ALT). Based on J-V and TEM analysis two degradation mechanisms can be discerned, one occurring at relatively low ALT temperatures and one occurring at higher ALT temperature. Initially the front contact microstructure of a solar cell consists of well defined GaAs, Au and Cu layers. After ALT at low temperatures (<250°C) the Au and Cu layers intermix, eventually forming a completely intermixed Au/Cu layer with a diffuse Cu layer on top of it. This intermixing process has no significant impact on the J-V characteristics of the solar cells, even after ALT of 55 days at 200°C (equal to 15 years at 100°C at an E_a of 0.70eV). At higher ALT temperatures (≥250°C) intermixing of Au and Cu occurs more rapidly and also recrystallization of the metals with the GaAs contact layer takes place, yielding an intermixed Au/Cu layer at the top of the contact with a recrystallized metal/GaAs layer having distinct grains and well defined grain boundaries below it. Eventually the GaAs contact layer (almost) completely recrystallizes with the metals until the recrystallization process is blocked by the AlInP window. Via the grain boundaries in this recrystallized layer, Cu atoms can diffuse rapidly into the active layers of the solar cell, where they introduce trap levels and cause a decrease in V_{oc}.

As the recrystallization process is highly unlikely to occur during operation in space, it is necessary that future experiments with both substrate based and thin-film cells are conducted at test temperatures well below 250°C so as to gain a better understanding of degradation at relatively low temperatures. As the intermixing between Au and Cu also occurs at low temperatures and appears to be the first step in the high temperature degradation process, a potential solution to Cu diffusion should be aimed at stabilizing this interface. This can be done either by replacement of Cu with a metal that forms a stable interface with Au or by introducing a diffusion barrier which forms stable interfaces with both Au and Cu.

Acknowledgements

The authors would like to thank Mr. W. Corbeek for the technical support. This project was financially supported by the Netherlands Space Office (NSO) under projectnumber PEP12010.

References

1 M. M. A. J. Voncken, J. J. Schermer, A. T. J. van Niftrik, G. J. Bauhuis, P. Mulder, P. K. Larsen, T. P. J. Peters, B. de Bruin, A. Klaassen and J. J. Kelly, *Journal of the Electrochemical Society*, 2004, **151**, G347.

2 A. T. J. van Niftrik, J. J. Schermer, G. J. Bauhuis, P. Mulder, P. K. Larsen and J. J. Kelly, *Journal of the Electrochemical Society*, 2007, **154**, D629.

3 R. Tatavarti, G. Hillier, A. Dzankovic, G. Martin, F. Tuminiello, R. Navaratnajarah, G. Du, D. P. Vu and N. Pan, 33rd IEEE Photovoltaics Specialists Conference, 2008, pp. 1–4.

4 G. J. Bauhuis, P. Mulder, E. J. Haverkamp, J. C. C. M. Huijben and J. J. Schermer, *Solar Energy Materials & Solar Cells*, 2009, **93**, 1488–1491.

5 G. J. Bauhuis, J. J. Schermer, P. Mulder, M. M. A. J. Voncken and P. K. Larsen, *Solar Energy Materials & Solar Cells*, 2004, **83**, 81–90.

6 J. J. Schermer, G. J. Bauhuis, P. Mulder, E. J. Haverkamp, J. van Deelen, A. T. J. van Niftrik and P. K. Larsen, *Thin Solid Films*, 2006, **511–512**, 645–653.

7 B. M. Kayes, H. Nie, R. Twist, S. G. Spruytte, F. Reinhardt, I. C. Kizilyalli and G. S. Higashi, Proceedings of the 37th IEEE

This journal is © The Royal Society of Chemistry [year]

Photovoltaics Specialists Conference, 2011.
8 O. D. Miller, E. Yablonovitch and S. R. Kurtz, *IEEE Journal of Photovoltaics*, 2012, **2**, 303–311.
9 J. J. Schermer, P. Mulder, G. J. Bauhuis, P. K. Larsen, G. Oomen and E. Bongers, *Progress in Photovoltaics: Research and Applications*, 2005, **13**, 587–596.
10 N. J. Smeenk, C. Mooney, J. Feenstra, P. Mulder, T. Rohr, C. O. A. Semprimoschnig, E. Vlieg and J. J. Schermer, *Polymer Degradation and Stability*, 2013, **98**, 2503–2511.
11 J. Feenstra, R. H. van Leest, N. J. Smeenk, P. Mulder, G. Oomen, E. Vlieg and J. J. Schermer, *submitted to Journal of Applied Polymer Science*, 2016, **-**, –.
12 G. J. Bauhuis, P. Mulder, E. J. Haverkamp, J. J. Schermer, E. Bongers, W. Köstler and G. Strobl, *Progress in Photovoltaics: Research and Applications*, 2010, **18**, 155–159.
13 J. Adams, V. Elarde, A. Hains, C. Stender, F. Tuminello, C. Youtsey, A. Wibowo and M. Osowski, *IEEE Journal of Photovoltaics*, 2013, **3**, 899–903.
14 M. M. A. J. Voncken, J. J. Schermer, G. J. Bauhuis, P. Mulder and P. K. Larsen, *Applied Physics A*, 2004, **79**, 1801–1807.
15 J. Yoon, S. Jo, I. S. Chun, I. Jung, H.-S. Kim, M. Meitl, E. Menard, X. Li, J. J. Coleman, U. Paik and J. A. Rogers, *Nature*, 2010, **456**, 329–334.
16 E. Grossman and I. Gouzman, *Nuclear Instruments and Methods in Physics Research B*, 2003, **208**, 48–57.
17 M.-C. Tseng, Y.-L. Horng, R.-H. andTsai, D.-S. Wuu and H.-H. Yu, *IEEE Electron Device Letters*, 2009, **30**, 940–942.
18 M.-C. Tseng, R.-H. Horng, F.-L. Wu, C.-H. Wu and M.-D. Yang, *IEEE Transactions on Electron Devices*, 2011, **58**, 3898–3904.
19 C. S. Fuller, J. D. Struthers, J. A. Ditzenberger and K. B. Wolfstirn, *Physical Review*, 1954, **93**, 1182–1190.
20 C. S. Fuller and J. C. Severiens, *Physical Review*, 1954, **96**, 21–25.
21 F. C. Frank and D. Turnbull, *Physical Review*, 1956, **104**, 617–618.
22 A. G. Tweet and C. J. Gallagher, *Physical Review*, 1956, **103**, 828.
23 C. S. Fuller and J. M. Whelan, *Journal of Physics and Chemistry of Solids*, 1958, **6**, 173–177.
24 R. N. Hall and J. H. Racette, *Journal of Applied Physics*, 1964, **35**, 379–397.
25 J. Blanc and L. R. Weisberg, *Journal of Physics and Chemistry of Solids*, 1964, **25**, 221–223.
26 C. S. Fuller, K. B. Wolfstirn and H. W. Allison, *Applied Physics Letters*, 1964, **4**, 48–49.
27 F. Hasegawa, *Journal of Applied Physics*, 1974, **45**, 1944–1947.
28 S. M. Sze and J. C. Irvin, *Solid-State Electronics*, 1968, **11**, 599–602.
29 H. J. Queisser and C. S. Fuller, *Journal of Applied Physics*, 1966, **37**, 4895–4899.
30 J. R. Davis Jr., A. Rohatgi, R. H. Hopkins, P. D. Blais, P. Rai-Choudhury, J. R. McCormick and H. C. Mollenkopf, *IEEE transactions on Electron Devices*, 1980, **27**, 677–687.
31 A. Rohatgi, J. R. Davis Jr., R. H. Hopkins, P. Rai-Choundhury, P. G. McMullin and J. R. McCormick, *Solid-State Electronics*, 1980, **23**, 415–422.
32 G. Coletti, P. C. P. Bronsveld, G. Hahn, W. Warta, D. Macdonald, B. Ceccarolo, K. Wambach, N. L. Quang and J. M. Fernandez, *Advanced Functional Materials*, 2011, **21**, 879–890.
33 H. Okamoto, D. J. Chakrabarti, D. E. Laughlin and T. B. Massalski, *Bulletin of Alloy Phase Diagrams*, 1987, **8**, 454–473.
34 C. T. Tsai and R. S. Williams, *Journal of Materials Research*, 1986, **1**, 352–360.
35 R. Schmid-Fetzer, *Journal of Electronic Materials*, 1988, **17**, 193–200.
36 C. Brandt, C. Baur, A. Caon, P. Müller-Buschbaum, C. Zimmermann and T. Andreev, *IEEE Journal of Photovoltaics*, 2013, **3**, 904–908.
37 R. H. van Leest, G. J. Bauhuis, P. Mulder, R. van der Heijden, E. Bongers, E. Vlieg and J. J. Schermer, *Solar Energy Materials & Solar Cells*, 2015, **140**, 45–53.
38 N. Núñez, J. R. González, M. Vázquez, C. Algora and P. Espinet, *Progress in Photovoltaics: Research and Applications*, 2013, **21**, 1104–1113.
39 M. Vázquez, C. Algora, I. Rey-Stolle and J. R. González, *Progress in Photovoltaics: Research and Applications*, 2007, **15**, 477–491.
40 J. R. González, M. Vázquez, N. Núñez, C. Algora, I. Rey-Stolle and B. Galiana, *Microelectronics Reliability*, 2009, **49**, 673–680.
41 P. Espinet-González, C. Algora, N. Núñez, V. Orlando, M. Vázquez, J. Bautista and K. Araki, *Progress in Photovoltaics: Research and Applications*, 2015, **23**, 559–569.
42 ESA-ESTEC Requirements & Standards Division, *ECSS-E-ST-20-08C, Space Engineering: Photovoltaic assemblies and components*, 2012.
43 M.-A. Nicolet, *Thin Solid Films*, 1978, **52**, 415–443.
44 E. Kinsbron, P. Gallagher and A. T. English, *Solid-State Electronics*, 1979, **22**, 517–524.